On-the-go hyperspectral imaging for the in-field estimation of grape berry soluble solids and anthocyanin concentration

Salvador Gutiérrez, Javier Tardaguila, Juan Fernández-Novales, Maria-Paz Diago*

Instituto de Ciencias de la Vid y del Vino (University of La Rioja, CSIC, Gobierno de La Rioja) Ctra. Burgos Km, 6, 26007 Logroño, Spain.

*Corresponding author: maria-paz.diago@unirioja.es, +34941299731

Abstract

Background and Aims

Hyperspectral imaging is a powerful tool for fruit composition monitoring, but it is mostly used under laboratory conditions. This work presents a new solution for the non-destructive, in-field prediction of total soluble solids and anthocyanin concentrations in wine grapes in the plant using on-the-go hyperspectral imaging.

Methods and Results

The acquisition of hyperspectral images was carried out under natural illumination conditions using a VIS-NIR hyperspectral camera (400-1000 nm) mounted on an all-terrain vehicle moving at 5 km/h on a commercial Tempranillo vineyard located in La Rioja, Spain. Measurements were taken in four different dates during the grape ripening of season 2017. Grape composition analyses were performed upon the measured grapes for the development of spectral prediction models trained with support vector machines. Total soluble solids models returned determination coefficients R^2 of 0.91 for a 5-fold cross validation (RMSE of 1.358 ºBrix) and 0.92 for the prediction of external samples (RMSE of 1.274 ºBrix). In the case of anthocyanin concentrations, R^2 of 0.72 was achieved for cross validation (RMSE of 0.282 mg/g berry) and 0.83 in prediction (RMSE of 0.211 mg/g berry). Additionally, spatial-temporal variation maps were developed for the four dates displaying the vineyard evolution during grape ripening.

Conclusions

The results support the actual capability of on-the-go hyperspectral imaging for the automated estimation of grape composition parameters directly in the field.

Significance of the Study

The on-the-go hyperspectral imaging methodology described in this study could be considered as a powerful tool for in-field applications in agriculture and vineyard unsupervised monitoring.

Keywords: svm, plant phenotyping, regression, sensors, proximal sensing

1 Introduction

Wine quality is directly affected by the compounds present in grapes (Kennedy 2010). The evaluation of grape ripening and quality is often performed by monitoring two important composition parameters: the total soluble solids (TSS) and, in the case of red grapes, the anthocyanin concentrations. TSS refers to the berry's primary metabolite, directly related to the alcoholic strength of the produced wines (Gomes et al. 2017). On the other hand, anthocyanin are phenolic compounds existing in red grape skins (Meléndez et al. 2013) which are responsible for skin tissue pigmentation and red wine color (Boulton 2001). Nowadays, these two grape compositional variables are crucial to determine optimal harvest time, and highly relevant to establish the grape price in many wineries and cooperatives worldwide (Bramley et al. 2011). Being both methods destructive, TSS can be quickly and easily measured using hand-held devices (refractometers), but anthocyanin concentration analysis requires complex wet chemistry methodologies (Iland 2004) that, although provide accurate results, are time consuming, need for specialized personnel and generate chemical waste (Liang et al. 2008). In this context, it may be very valuable for the wine industry to have fast, easy to operate, robust, nondestructive methods to assess the berry composition and its evolution along grape ripening.

On the other hand, knowledge of the spatial-temporal variation of the TSS and anthocyanin contents within a vineyard may assist decision making regarding sampling and vineyard management, especially if selective harvest is aimed. As a matter of fact, the pattern of spatial variability of grape anthocyanins in a Tempranillo vineyard was shown to change with phenology (Baluja, Diago, Balda, et al. 2012, Baluja, Diago, Goovaerts, et al. 2012). Therefore, to have a truthful picture of the spatial-temporal dynamics of grape composition evolution during ripening in a vineyard, a huge amount of measurements at different timings and spatial positions are required. Unfortunately, the quick in-field measurement of a huge number of samples is very hard for TSS and impossible in the case of analyzing anthocyanin concentrations.

Several applications can be found in the literature for the in-field manual monitoring of grape composition (Ben Ghozlen et al. 2010, Baluja, Diago, Goovaerts, et al. 2012, Barnaba et al. 2014), but these are still time and labor intensive, therefore unsuited for the retrieval of a large and representative amount of data. Also, remote sensing has been attempted as a non-destructive alternative to appraise the spatial variability of grape colour in the vineyard. However, spectral indices were found to be weakly correlated with grape anthocyanins (Lamb et al. 2004). Other authors mounted a chlorophyll-based sensor above the discharge conveyor of a tow-behind harvest machine to determine the anthocyanin content of the harvested fruit at georeferenced spatial positions within the vineyard (Bramley et al. 2011). This enabled the characterization of the vineyard's spatial variability of grape anthocyanins but since assessment was done after the fruit was picked, no possibility of selective harvest decision was provided.

To overcome these limitations, ground-based on-the-go monitoring can be seen as the next natural step from in-field, manual data collection from the crops. Nevertheless, the on-the-go approach presents several pitfalls that have impeded the transition of successful techniques using manual measurements (Ghozlen et al. 2010) to the continuous monitoring from moving vehicles. Among these restraints, a) the need to "see" the grapes; that is the necessity of having sufficient amount of exposed fruit for the sensor to target fruit instead of material other than grapes; b) the small measuring spot area of many devices (e.g. ~3 cm^2, Fernández-Novales et al. 2017) which make difficult to hit on fruit material; or c) the insufficient signal to noise intensity of many devices, when operated contactless at several cm from the targeted canopy. Moreover, the continuous acquisition of data entails a higher resolution monitoring, and the generation of a big amount of data, which need to be handled and analysed using novel methods.

In the context of precision agriculture, the relentless development of new sensors, especially within spectral technology, allows for the massive acquisition of high resolution data that could be very useful for the monitoring of crop features, such as grape composition, that can be key in decision-making for selective harvest or winemaking operations. For this reason, the use of on-the-go spectroscopy under field conditions needs to be studied in order to bring its high potential into in-field agricultural applications.

In the last years, hyperspectral imaging (HSI) has arisen as a powerful technology for the non-destructive analysis in several agricultural and food quality and safety applications (Sun 2010,

Park & Lu 2015). HSI combines into a single tool the features of two different fields: the potential of spectroscopy modeling and the spatial nature of two-dimensional digital imaging. As each pixel in a hyperspectral image provides the full spectrum from the measured target, the capability of this technology for the massive extraction of information from that target raises it as a powerful tool to be employed in the industry. HSI has been widely applied to successfully estimate fruit composition. HSI-based modeling for the TSS prediction has been recently studied in grape berries (Gomes et al. 2017, Piazzolla et al. 2017), apple (Ma et al. 2017, Mo et al. 2017, Tian et al. 2018) or mango (Rungpichayapichet et al. 2017), while the anthocyanin concentrations has been predicted also in grape berries (Diago et al. 2016, Martínez-Sandoval et al. 2016, Zhang et al. 2017), mulberry (Huang et al. 2017) or raspberry (Rodríguez-Pulido et al. 2017). Nevertheless, all these works (and almost every other fruit-related studies using HSI) have one important factor in common: all they were performed in laboratory, under controlled conditions, such as illumination, sample positioning and temperature, among others. It is thus a natural next stage to study how a HSI system behaves when it is deployed in the field, but great challenges arise with this apparently small step. Different ambient conditions are a constant during in-field experiments, and also target's location and position are non-constant features either. For this reason, there is room for many potential applications of HSI in the field, and for studying new methodologies for the automated acquisition and processing of hyperspectral images. Very few works can be found in the literature using in-field HSI (Deery et al. 2014, Williams et al. 2017), but even on-the-go approaches in robotics has been reported (Underwood et al. 2017, Wendel & Underwood 2017). Given the demonstrated potential of HSI for the prediction of grape composition parameters, the addition of a higher level of vineyard monitoring that can be obtained by on-the-go measurements opens a new frontier in precision viticulture, as high-resolution information can be obtained, processed and mapped using automated platforms.

For these reasons, the development of a new methodology for the in-field monitoring of grape composition parameters is a desirable next step in the context of precision viticulture and wine decision making, and new technologies makes this an attainable objective. Therefore, the goal of this work was the in-field estimation and mapping of two important grape composition parameters, TSS and anthocyanin concentrations, with the clusters still in the plants, using non-destructive on-the-go hyperspectral imaging.

2 Materials and methods

The design of the study was split into three major stages (Fig. 1). In the first one, the in-field experiments were carried out, comprising the on-the-go HSI image acquisition and the collection and chemical analyses of the imaged grape samples. In the second stage, the hyperspectral images were processed (for the automated extraction of grape berry spectra) and the datasets generated. In the last stage, the dataset was used as input for the training of different prediction models using machine learning algorithms and use for the generation of different maps.

2.1 In-field experiments

2.1.1 Experimental layout

The experiment was performed in a 0.7 ha commercial vineyard located in Ábalos, La Rioja, Spain (Lat. 42º 34' 45.7", Long. -2º 42' 27.78", Alt. 628 m). Grapevines of Tempranillo (*Vitis vinifera* L.) variety were planted in 2010, on rootstock R-110 and trained to a vertically shoot-positioned (VSP) trellis system. The rows in the vineyard had a Northeast-Southwest orientation, and 2.20×1.00 meters inter and intra row distances. Three different equally-distanced rows were selected and, within each one of them, 12 blocks with five plants each (five meters per block) were chosen for the spectral and grape berry analyses (a total of 36 blocks). Hyperspectral measurements were performed on the east side of the canopy, which was defoliated on the basal zone. In order to modeling all different stages of ripening, data acquisition was carried out during four dates from veraison to harvest, in different phenological stages—according to the modified Eichhorn and Lorenz system (Coombe 1995)—during season 2017: 11 August, stage 36; 24 August, stage 37; 18 September, stage 38; and 28 September, stage 38. Therefore, the total number of blocks that were measured throughout the entire experiment was 144 (36 blocks per date, four different dates).

Hyperspectral images were acquired on-the-go using a push broom Resonon Pika L VNIR hyperspectral imaging camera (Resonon, Inc., Bozeman, MA, USA) that was installed on an all-terrain vehicle ATV, Fig 2) (Trail Boss 330, Polaris Industries, MN, USA) and connected

158 to an industrial computer. The camera's spectral resolution was 2.1 nm (300 bands from 400 to
159 1000 nm), with 300 pixels of spatial resolution. An 8 mm focal length lens was used, pointed
160 to the canopy on a lateral point of view at 2.0 m of distance, that cast a vertical recording line
161 upon the plants of 1.32 m (field of view of 36.5°). The recording line covered the whole vine
162 canopy, including the fruiting zone (Fig. 2). The 36 measurements per day (one for each block)
163 were performed on the southeast canopy side, between 10:00 and 14:00, under the natural
164 illumination from the sun only. To test the HSI methodology under reproducible scenarios (*i.e.*,
165 other different kinds of terrestrial vehicles), no specific mechanical compensation was applied
166 for terrain irregularities corrections other than vehicle's own suspension. Nevertheless, the
167 distance between camera and plants made it certain that the scene acquired by the sensor always
168 covered the whole plants (and, therefore, the grape bunches).

169 To take into account the naturally variable illumination conditions, the values for the camera
170 configuration parameters (integration time and frames per seconds, FPS) were adapted for each
171 block measurement, depending on the light intensity, in order to find the best trade-off between
172 acceptable image composition, enough spectral intensity and the prevention of saturation. FPS
173 ranged from 50 (taking one frame each 20 milliseconds) at the beginning of the season to 40 at
174 the end (one frame each 25 milliseconds). Prior to the block's hyperspectral measurement, a
175 Spectralon® white reference (a surface with a reflectance over 95%) was manually presented
176 to the camera and recorded simulating the same position and distance than to the canopy. A
177 dark current measurement was also performed, to obtain the inherent electronic noise. After
178 this, the block was imaged on-the-go at a constant speed of 5 km/h, composing a hyperspectral
179 image by push broom scanning (Fig. 2) with an average number of scanlines (columns) of 710,
180 with 900 pixels each one. On average, a total of 639,000 pixels (*i.e.*, spectra) per block were
181 acquired.

182 The spectral light intensity values collected by the camera were translated into reflectance (R):

183 $$R = \frac{G(\lambda) - D(\lambda)}{W(\lambda) - D(\lambda)}$$

184 where λ is a wavelength, G is the intensity of the light reflected by the canopy, W is the intensity
185 of the light coming from the white reference, and D is the dark current. The reflectance was
186 then converted into absorbance (log (1/R)). To prevent the noise that is commonly found in the
187 tails of a spectral signal, the first 10 bands and the last 50 ones were discarded, thus obtaining
188 spectra that comprised 240 bands (from 410 to 921 nm).

Hyperspectral images were georeferenced using a GPS receiver Ag Leader 6500 (Ag Leader Technology, Inc., Ames, IA, USA) with RTK correction installed on the ATV.

2.1.2 Analysis of grape composition

At each measuring date, immediately after the HSI of each block, all the exposed clusters were identified and, from them, portions of 10-15 visible berries were manually picked, bagged and labeled for their subsequent chemical analysis. On average, a total of 200 grape berries per block were collected each date. The closed bags that contained the berries were then transported in portable refrigerators to the laboratory and stored in a freezer at -20 ºC until chemical analysis.

Two different grape berry composition parameters were measured: the total soluble solid (TSS) and total anthocyanin concentrations. Fruits were thawed overnight (in a cold room at 4ºC) before grape composition analysis. For each sample, a subsample of 100 berries was hand crushed and filtered. The TSS concentration was determined using a temperature compensating digital refractometer Quick-Brix 60 (Mettler Toledo, LLC, Columbus, OH, USA), expressed as ºBrix. The remaining berry sub-sample was homogenized using a high-performance disperser T25 Ultra-Turrax (IKA, Staufen, Germany) at high speed (14,000 rpm for 60 s). Afterwards, anthocyanin concentrations were measured (Iland 2004) and expressed as mg per gram of berry mass.

2.2 Image processing

2.2.1 Processing of hyperspectral images

From each hyperspectral image, it was needed to automatically obtain all the spectra belonging to grape clusters. To do this, prior to the automated image processing, a grape reference spectrum was obtained by manually selecting grape spectra from all the images (regions of approximately 200 spectra) and then averaging them. With this signature spectrum (that was also pre-processed with a Saviztky-Golay smoothing and derivative (Savitzky & Golay 1964)), the following described algorithm was coded using Python 3.6.1:

Defining *I* as the original hyperspectral image and *C* an empty matrix with the same width and height than *I*. Each one of the bins of *C* (with coordinates *x*, *y*) is filled with the determination coefficient from the correlation analysis between each one of the pixels of *I* in the same position (*e.g.*, spectra in the *x*, *y* coordinates) and the grape signature spectra. The similarity of each pixel (spectrum) from *I* with the grape signature spectra is thus represented as a R^2 value, and a correlation matrix *C* is built with them. After a two-dimensional Gaussian smoothing to *C* (with σ set to 1.0), all the pixels from *C* that surpass the 0.75 mark are identified as grape spectra and averaged (the 0.75 value was manually selected after intensive supervised review of the results of the processing of several hyperspectral images). This average is thus considered as the image (block) grape average spectrum. For more details, the reader is referred to the pseudocode description of this algorithm included as supplementary material.

Fig. 3 exemplifies the output of this algorithm. In (a), the original hyperspectral image is displayed with the RGB channels, while in (b), its correlation matrix *C* after the Gaussian smoothing is shown. Finally, the selected grape pixels (those from *C* whose R^2 are equal or greater than 0.75) are segmented in (c).

In a small proportion of hyperspectral images, a very small number of pixels identified as grape had a spectral shape with higher intensity than the white reference's. This was due to incident sunlight that was directly reflected into the camera's sensor, hence returning a reflectance value over 1.0 in some wavelengths. These pixels were therefore discarded from the final spectra averaging.

2.2.2 Generation of the dataset

After the grape berry spectra and the chemical parameters were obtained for each block, they were used to build the dataset, in which each spectrum was linked with its corresponding composition parameters. Having 36 blocks and four different measurement dates, the dataset comprised a total of 144 samples, covering all the measurement dates. From this, train and test subsets were built in an 80-20 ratio respectively by randomly extracting a 20% of samples per date, making up a train set of 115 samples and a test set of 29 samples.

2.3 Development of prediction models

2.3.1 Machine learning modeling

Several machine learning algorithms were tested for modeling, based on authors' experience and criteria, and Epsilon-Support vector machines (ε-SVMs) were finally used for the training of the regression models due to its better performance statistics. The input independent variables X were the spectra ($|X| = 240$, the number of spectral bands), pre-processed with standard normal variate (Barnes et al. 1989) and Savitzky-Golay filter (second-grade derivative, window size of 15), while the TSS and anthocyanin concentrations were used as dependent variables y, each one for the training of two different models. In both cases, a radial basis function kernel was used, with $\varepsilon = 0.1$ and $\gamma = 0.00417$ ($1/|X|$). The penalty parameter C was set to 100 in the case of TSS and 30 for anthocyanin concentrations. The performance of SVM for the train test was evaluated using a 5-fold cross validation. The prediction results were obtained by training a model with all the samples from the train test and predicting the samples from the test set. All the models were developed using the Epsilon-Support vector regression implementation in scikit-learn 0.18.1 (Pedregosa et al. 2011).

2.3.2 Spatio-temporal mapping

The usefulness of on-the-go HSI for the monitoring of grape composition within a vineyard was illustrated by developing TSS and anthocyanin concentrations prediction maps from the commercial vineyard in which the experiments were performed during the ripening period. Interpolation maps were generated using multilevel b-spline interpolation (Lee et al. 1997) implemented in QGIS 2.19 (Free Software Foundation, Boston, MA, USA).

3 Results

3.1 Grape composition variation

The histograms for TSS and anthocyanin concentrations on each experimental date are displayed in Fig. 4, also summarizing the main statistical information about the variation of these two compositional parameters.

TSS yielded a wide range from 10.7 ºBrix (expected value for grapes at mid-ripening phenological stage) to 25.2 ºBrix, indicating that the grapes reached full maturity. The mean and standard deviation values also indicated a wide variability within the measured TSS values. The results from the anthocyanin analyses demonstrated that the same behavior was observed for this parameter, with values ranging from lower values of 0.05 (at veraison, when anthocyanin synthesis has not yet been triggered in all berries) to 2.01 mg/g berry at harvest. The mean values increased throughout the season, while the standard deviations widened until September.

Attending to the shape of the histograms, as expected for both parameters, the gross of their values per date increased as season evolved. For TSS, very similar values were found in the two last dates, indicating a final stage in maturity at which TSS no longer increases by physiological ripening process. In the case of the anthocyanin concentrations, the values for the first date stayed within a limited mg/g berry range, but this range became wider in the next three dates, a behavior that could correspond to an asynchronous ripening of the fruit (internal variability).

3.2 Prediction models and mapping

The cross-validation and prediction results of the total soluble solids models are plot in Fig. 5. The 5-fold cross validation (Fig. 5(a)) yielded a determination coefficient R^2 of 0.91, with a root mean squared error (RMSE) of 1.358 ºBrix. The regression line can be found almost exactly over the 1:1 line, and a good distribution of the samples along it was observed. The prediction results (Fig. 5(b)) cast comparable values for both R^2 (0.92) and RMSE (1.274 ºBrix).

Fig. 6 gathers the regression plots from the cross validation and prediction models for the berry anthocyanin concentrations. Fig. 6(a) displays a cross validation R^2 of 0.72, while the prediction results (Fig. 6(b)) yielded a larger determination coefficient of 0.83. For the first case, the RMSE value was 0.282 mg/g berry, but, in Fig. 6(b), the lower number of samples and their concentrated locations reduced the RMSE value to 0.211 mg/g berry.

In Fig. 7, the evolution of TSS and anthocyanin concentrations are displayed in eight prediction maps, one per date and grape composition parameter, for the commercial vineyard plot in which the experiments were carried out. The evolution of TSS (Fig. 7) remained steady throughout the different maturity stages, and a large gap can be found between 24 August and 18 September. The maximum values were reached in the latter, and in the last date only a slight increase in ºBrix was found. The south corner of the vineyard plot showed the quickest ripening speed.

In the case of the anthocyanin concentrations, big gaps were present between the four dates, from little variation (from 0.15 to 0.35 mg/g berry) on 11 August, to a plot with higher anthocyanin concentrations and variability on 28 September.

3.3 Computational cost

The processing of 36 hyperspectral images using the described algorithm in section 2.2.1 took, per date, an average of 5 hours and 35 minutes in an Intel® Core™ i7-5820K CPU with 16 GB of RAM (no thread optimization). Taking into account that each image was composed of approximately 710 scanlines (columns), the calculations result in an average processing time of 0.79 s per column, while the prediction of a single sample using a trained SVM model took 0.05 s. With all this, on a real-time scenario, the processing and prediction of a hyperspectral scanline would take less than a second.

4 Discussion

The present work has displayed a new solution for the non-destructive, in-field estimation of grape composition using on-the-go hyperspectral imaging in a commercial vineyard. These results have demonstrated not only the suitability of hyperspectral cameras for the estimation of two important grape composition parameters, but the actual possibility of bringing this kind of devices from in-door to the field. HSI is a technology originally conceived to be employed in laboratories or in-door environments, in which the environmental conditions can be completely controlled, in terms of illumination, temperature, sample and camera stability, etc. Nevertheless, its passage to the field requires the overcoming of the changing conditions caused

by these factors. Additionally, in this work, the on-the-go acquisition of hyperspectral images successfully carried out, by means of a motorized platform at agricultural speeds (5 km/h). The use of a mobile vehicle brings specific circumstances that are not contemplated in in-door conditions (or even outdoor ones, but with static measurements), such as irregularities in the terrain, motor vibrations, slight but constant differences in the distance between the lens and the target, heterogeneous speed, etc. The presented results, one of the first attempts---and, to the best of our knowledge, the first one in grapevine---validate a feasible methodology for the development of fruitful prediction models using a hyperspectral camera within all the mentioned conditions. This opens a wide number of options for the monitoring of a vineyard, by different mobile platforms.

The methodologies studied in this work are prone to be deployed on specific, man-driven platforms (like the ATV used), agricultural vehicles operating upon the crops, or even using autonomous phenotyping and monitoring platforms (*i.e.*, agricultural robots). This last option also requires an important step of automation in the image computation, something that can be achieved when dealing with hyperspectral images, as the methodology described in section 2.2.1 (the precise selection of grape spectra and the prediction of their composition value) could be directly translated even into a robot. A collection of grape spectral could be preloaded into the platform's system, limiting the manual grape sample spectra collection to, for example, once per season. Therefore, along with a pretrained model, the prediction of grape composition could be fully automated during plot monitoring by the platform. Some works in the literature have proven that HSI can be performed under field conditions (Williams et al. 2017) and even on-the-go (Deery et al. 2014, Underwood et al. 2017, Wendel & Underwood 2017). It could be possible the development of a complete integration between HSI sensors, GPS and computing into a single platform capable of performing real-time assessment in the vineyard. Some recent examples have been published using HSI devices with integrated GPS (Sandino et al. 2018, Vanegas et al. 2018). This scheme is valid for its integration within current viticulture-related work trends, and it can be possible to take advantage of working agricultural vehicles already deployed and to install a HSI monitoring system on them. The exposed outcomes of in-field, on-the-go HSI open new windows for its usage in many other different crops, using similar techniques for spectral segmentation and prediction model training. Additionally, and taking advantage of HSI's extra spatial dimensions, the use of this technology is not limited for the automatic monitoring of just the fruit, but also other organs at the same time (*e.g.*, leaves or stems).

Several works have demonstrated that the monitoring of grape composition throughout the ripening is a feasible goal using spectroscopic technologies (Larrain et al. 2008, Cao et al. 2010, González-Caballero et al. 2010, Bellincontro et al. 2011, Barnaba et al. 2014, Musingarabwi et al. 2016), performed mostly under laboratory conditions. In-field grape composition monitoring has been reported in previous works using spectroscopy, but from contact, discrete measurements using portable manual devices. A portable NIR spectrophotometer was used for the estimation of TSS under field conditions (Urraca et al. 2016), reporting prediction RMSE values of 1.68 ºBrix and 10-fold cross validation laboratory R^2 up to 0.90 (with an RMSE of 1.47 ºBrix). These results were slightly lower than those from the present study, but still comparable, as a portable device can be easily deployed in the field. Nevertheless, clear advantages of on-the-go HSI can be found, as the combination of fastest acquisition time and larger number of samples covered makes the detailed monitoring of a whole vineyard plot a more feasible goal. Staying on this subject, HSI has been previously proven to be an accurate tool for TSS and anthocyanin concentrations estimation under laboratory conditions. Regarding TSS, several works have reported prediction R^2 values from 0.88 to 0.93 (RMSEs of 0.950 and 0.930 ºBrix, respectively) (Gomes et al. 2017, Piazzolla et al. 2017). Similar performance values were obtained for ºBrix prediction using the on-the-go approach described in this study, possibly explained by the fact that the same VIS-NIR spectral region (400-1000 nm) was used. Regarding the estimation of grape anthocyanin concentrations, HSI has been widely employed for this goal (Diago et al. 2016, Martínez-Sandoval et al. 2016, Zhang et al. 2017). The reported R^2 values range from 0.72 up to 0.93, in line with the ones presented in this study. It must be highlighted that, if the prediction models developed in this work can be deemed to be solid and reliable, it is also because the in-field spectral information used for their training came from four different dates and phenological stages. Pre-veraison data acquisition was considered, but rapidly discarded since biosynthesis or changes in composition of most relevant grape berry compounds start at veraison. Moreover, it is at this stage when the vine's vegetative growth stops, therefore the most prominent sinks in the plant are the berries, hence the changes in their composition. From a practical perspective (not scientifically speaking) there is no interest in assessing the berry composition prior to veraison, as no utilization for winemaking can be done at those early stages. For these reasons, including data from dates before veraison would not improve results, nor would it be useful for vineyard monitoring. However, the training with data from different post-veraison phenological phases made thus possible for the models to acquire the capability of monitoring the evolution and spatial distribution of total soluble solids and anthocyanin concentrations at different moments along grape ripening. This feature

increases the application value of the models developed using the described methodology in commercial and industrial environments.

The on-the-go estimation of important grape composition parameters brings a new tool for many actors in grapevine growing and wine industry. The developed HSI methodology has proven to overcome two of the three main limitations for on-the-go grape monitoring, that is a larger spot size of measurement (basically all fruit exposed area is measured) and the sufficient signal to noise ratio. Regarding the need to "see the fruit", some level of cluster exposure in undoubtedly required, but partial basal defoliation of the morning side mainly, is a common practice in many regions worldwide to improve cluster exposure and air circulation (Smart et al. 1991).

The mapping of a whole vineyard plot perfectly fits with the goal of precision viticulture, in the current sustainability context, as the accurate monitoring and characterization of heterogeneous zones carries a high amount of useful information that could help in the decision-making process. TSS estimation is directly related to the monitoring of grape ripening, allowing to take precise decisions on when and where to harvest, while anthocyanin concentrations could for example help to characterize zones of different grape qualities, assigning them to different wine-making processes. As exposed in Fig. 7, the monitoring and mapping of composition parameters lets the visualization of their spatial distribution within the field. In this case, at each measured stage during grape ripening, the plotted results from this methodology can be used as a powerful diagnostic tool, improving and optimizing the decision-making capacities.

5 Conclusions

This work presents the potential of in-field on-the-go hyperspectral imaging for the monitoring of grape composition in a commercial vineyard. The results obtained from the spectral models trained with support vector machines demonstrates that it is possible to deploy a hyperspectral camera from the laboratory to the field, that can acquire high resolution information of large areas in a fast, unsupervised approach. A HSI system could thus be attached to agricultural machinery or even robotics. Likewise, mapping of grape composition during different phenological stages in a season were developed, maps that provide the farmer with information that could be very useful in the decision making process. This work is also one of the few new applications of on-the-go HSI under field conditions, and possibly the first one in grapevine.

6 References

Baluja, J., Diago, M.P., Balda, P., Zorer, R., Meggio, F., Morales, F. and Tardaguila, J., (2012) Assessment of vineyard water status variability by thermal and multispectral imagery using an unmanned aerial vehicle (UAV). Irrig. Sci. **30**, 511–522.

Baluja, J., Diago, M.P., Goovaerts, P. and Tardaguila, J., (2012) Spatio-temporal dynamics of grape anthocyanin accumulation in a Tempranillo vineyard monitored by proximal sensing. Aust. J. Grape Wine Res. **18**, 173–182.

Barnaba, F.E., Bellincontro, A. and Mencarelli, F., (2014) Portable NIR-AOTF spectroscopy combined with winery FTIR spectroscopy for an easy, rapid, in-field monitoring of Sangiovese grape quality. J. Sci. Food Agric. **94**, 1071–1077.

Barnes, R.J., Dhanoa, M.S. and Lister, S.J., (1989) Standard normal variate transformation and de-trending of near-infrared diffuse reflectance spectra. Appl. Spectrosc. **43**, 772–777.

Bellincontro, A., Cozzolino, D. and Mencarelli, F., (2011) Application of NIR-AOTF spectroscopy to monitor Aleatico grape dehydration for Passito wine production. Am. J. Enol. Vitic. ajev--2010.

Boulton, R., (2001) The copigmentation of anthocyanins and its role in the color of red wine: a critical review. Am. J. Enol. Vitic. **52**, 67–87.

Bramley, R.G. V, Le Moigne, M., Evain, S., Ouzman, J., Florin, L., Fadaili, E.M., Hinze, C.J. and Cerovic, Z.G., (2011) On-the-go sensing of grape berry anthocyanins during commercial harvest: development and prospects. Aust. J. Grape Wine Res. **17**, 316–326.

Cao, F., Wu, D. and He, Y., (2010) Soluble solids content and pH prediction and varieties discrimination of grapes based on visible--near infrared spectroscopy. Comput. Electron. Agric. **71**, S15--S18.

Coombe, B.G., (1995) Growth stages of the grapevine: adoption of a system for identifying grapevine growth stages. Aust. J. Grape Wine Res. **1**, 104–110.

Deery, D., Jimenez-Berni, J., Jones, H., Sirault, X. and Furbank, R., (2014) Proximal remote sensing buggies and potential applications for field-based phenotyping. Agronomy **4**, 349–

379.

Diago, M.P., Fernández-Novales, J., Fernandes, A.M., Melo-Pinto, P. and Tardaguila, J., (2016) Use of visible and short-wave near-infrared hyperspectral imaging to fingerprint anthocyanins in intact grape berries. J. Agric. Food Chem. **64**, 7658–7666.

Fernández-Novales, J., Tardaguila, J., Gutiérrez, S., Marañón, M. and Diago, M.P., (2017) In field quantification and discrimination of different vineyard water regimes by on-the-go NIR spectroscopy. Biosyst. Eng.

Ghozlen, N. Ben, Cerovic, Z.G., Germain, C., Toutain, S. and Latouche, G., (2010) Non-destructive optical monitoring of grape maturation by proximal sensing. Sensors **10**, 10040–10068.

Gomes, V.M., Fernandes, A.M., Faia, A. and Melo-Pinto, P., (2017) Comparison of different approaches for the prediction of sugar content in new vintages of whole Port wine grape berries using hyperspectral imaging. Comput. Electron. Agric. **140**, 244–254.

González-Caballero, V., Sánchez, M.-T., López, M.-I. and Pérez-Marín, D., (2010) First steps towards the development of a non-destructive technique for the quality control of wine grapes during on-vine ripening and on arrival at the winery. J. Food Eng. **101**, 158–165.

Huang, L., Zhou, Y., Meng, L., Wu, D. and He, Y., (2017) Comparison of different CCD detectors and chemometrics for predicting total anthocyanin content and antioxidant activity of mulberry fruit using visible and near infrared hyperspectral imaging technique. Food Chem. **224**, 1–10.

Iland, P., (2004) Chemical Analysis of grapes and wine. Patrick Iland Wine Promotions PTYLTD.

Kennedy, J.A., (2010) Wine colour, in: Reynolds, A.G. (Ed.), Managing Wine Quality: Viticulture and Wine Quality. Cambridge: Woodhead Publishing, pp. 73–104.

Lamb, D.W., Weedon, M.M. and Bramley, R.G. V, (2004) Using remote sensing to predict grape phenolics and colour at harvest in a Cabernet Sauvignon vineyard: Timing observations against vine phenology and optimising image resolution. Aust. J. Grape Wine Res. **10**, 46–54.

Larrain, M., Guesalaga, A.R. and Agosín, E., (2008) A multipurpose portable instrument for determining ripeness in wine grapes using NIR spectroscopy. IEEE Trans. Instrum. Meas.

57, 294–302.

Lee, S., Wolberg, G. and Shin, S.Y., (1997) Scattered data interpolation with multilevel B-splines. IEEE Trans. Vis. Comput. Graph. **3**, 228–244.

Liang, Z., Wu, B., Fan, P., Yang, C., Duan, W., Zheng, X., Liu, C. and Li, S., (2008) Anthocyanin composition and content in grape berry skin in Vitis germplasm. Food Chem. **111**, 837–844.

Ma, T., Li, X., Inagaki, T., Yang, H. and Tsuchikawa, S., (2017) Noncontact evaluation of soluble solids content in apples by Near-infrared hyperspectral imaging. J. Food Eng.

Martínez-Sandoval, J.R., Nogales-Bueno, J., Rodríguez-Pulido, F.J., Hernández-Hierro, J.M., Segovia-Quintero, M.A., Martínez-Rosas, M.E. and Heredia, F.J., (2016) Screening of anthocyanins in single red grapes using a non-destructive method based on the near infrared hyperspectral technology and chemometrics. J. Sci. Food Agric. **96**, 1643–1647.

Meléndez, E., Ortiz, M.C., Sarabia, L.A., Íñiguez, M. and Puras, P., (2013) Modelling phenolic and technological maturities of grapes by means of the multivariate relation between organoleptic and physicochemical properties. Anal. Chim. Acta **761**, 53–61.

Mo, C., Kim, M.S., Kim, G., Lim, J., Delwiche, S.R., Chao, K., Lee, H. and Cho, B.-K., (2017) Spatial assessment of soluble solid contents on apple slices using hyperspectral imaging. Biosyst. Eng. **159**, 10–21.

Musingarabwi, D.M., Nieuwoudt, H.H., Young, P.R., Eyéghè-Bickong, H.A. and Vivier, M.A., (2016) A rapid qualitative and quantitative evaluation of grape berries at various stages of development using Fourier-transform infrared spectroscopy and multivariate data analysis. Food Chem. **190**, 253–262.

Park, B. and Lu, R., (2015) Hyperspectral imaging technology in food and agriculture. Springer.

Pedregosa, F., Varoquaux, G., Gramfort, A., Michel, V., Thirion, B., Grisel, O., Blondel, M., Prettenhofer, P., Weiss, R., Dubourg, V., Vanderplas, J., Passos, A., Cournapeau, D., Brucher, M., Perrot, M. and Duchesnay, E., (2011) Scikit-learn: Machine Learning in {P}ython. J. Mach. Learn. Res. **12**, 2825–2830.

Piazzolla, F., Amodio, M.L. and Colelli, G., (2017) Spectra evolution over on-vine holding of Italia table grapes: prediction of maturity and discrimination for harvest times using a Vis-NIR hyperspectral device. J. Agric. Eng. **48**, 109–116.

Rodríguez-Pulido, F.J., Gil-Vicente, M., Gordillo, B., Heredia, F.J. and González-Miret, M.L., (2017) Measurement of ripening of raspberries (Rubus idaeus L) by near infrared and colorimetric imaging techniques. J. Food Sci. Technol. **54**, 2797–2803.

Rungpichayapichet, P., Nagle, M., Yuwanbun, P., Khuwijitjaru, P., Mahayothee, B. and Müller, J., (2017) Prediction mapping of physicochemical properties in mango by hyperspectral imaging. Biosyst. Eng. **159**, 109–120.

Sandino, J., Pegg, G., Gonzalez, F. and Smith, G., (2018) Aerial Mapping of Forests Affected by Pathogens Using UAVs, Hyperspectral Sensors, and Artificial Intelligence. Sensors **18**, 944.

Savitzky, A. and Golay, M.J.E., (1964) Smoothing and differentiation of data by simplified least squares procedures. Anal. Chem. **36**, 1627–1639.

Smart, R., Robinson, M. and others, (1991) Sunlight into wine: a handbook for winegrape canopy management. Winetitles.

Sun, D.-W., (2010) Hyperspectral imaging for food quality analysis and control. Elsevier.

Tian, X., Li, J., Wang, Q., Fan, S. and Huang, W., (2018) A bi-layer model for nondestructive prediction of soluble solids content in apple based on reflectance spectra and peel pigments. Food Chem. **239**, 1055–1063.

Underwood, J., Wendel, A., Schofield, B., McMurray, L. and Kimber, R., (2017) Efficient in-field plant phenomics for row-crops with an autonomous ground vehicle. J. F. Robot. **34**, 1061–1083.

Urraca, R., Sanz-Garcia, A., Tardaguila, J. and Diago, M.P., (2016) Estimation of total soluble solids in grape berries using a hand-held NIR spectrometer under field conditions. J. Sci. Food Agric. **96**, 3007–3016.

Vanegas, F., Bratanov, D., Powell, K., Weiss, J. and Gonzalez, F., (2018) A novel methodology for improving plant pest surveillance in vineyards and crops using UAV-based hyperspectral and spatial data. Sensors **18**, 260.

Wendel, A. and Underwood, J., (2017) Illumination compensation in ground based hyperspectral imaging. ISPRS J. Photogramm. Remote Sens. **129**, 162–178.

Williams, D., Britten, A., McCallum, S., Jones, H., Aitkenhead, M., Karley, A., Loades, K.,

559 Prashar, A. and Graham, J., (2017) A method for automatic segmentation and splitting of
560 hyperspectral images of raspberry plants collected in field conditions. Plant Methods **13**,
561 74.

562 Zhang, N., Liu, X., Jin, X., Li, C., Wu, X., Yang, S., Ning, J. and Yanne, P., (2017)
563 Determination of total iron-reactive phenolics, anthocyanins and tannins in wine grapes of
564 skins and seeds based on near-infrared hyperspectral imaging. Food Chem. **237**, 811–817.

565

Figure legends

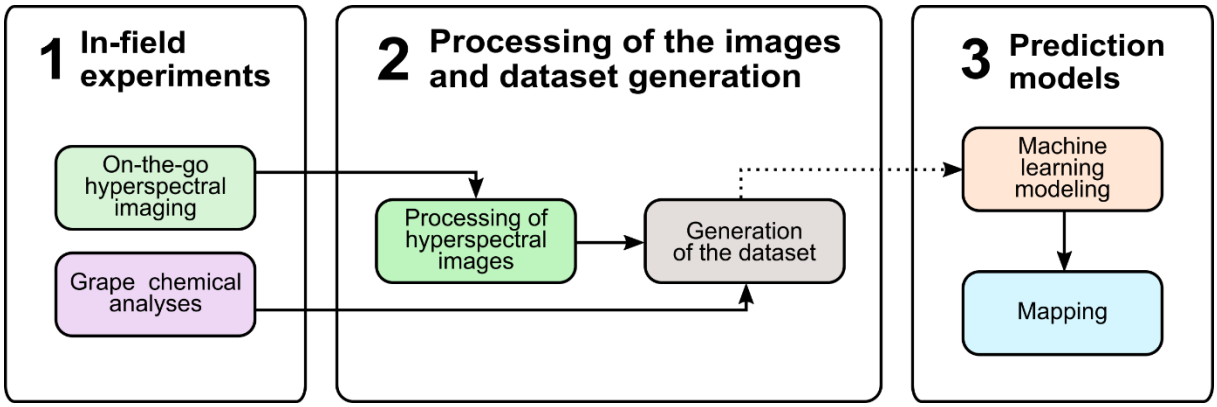

Fig 1 Design of the study, split into three major stages: in-field experiments, processing of the images and development of prediction models.

Fig 2 On-the-go hyperspectral imaging with a camera mounted on an ATV at 5 km/h. Images of the entire vine canopy were obtained from the ATV's motion, by push-broom scanning, and used for the estimation of grape composition.

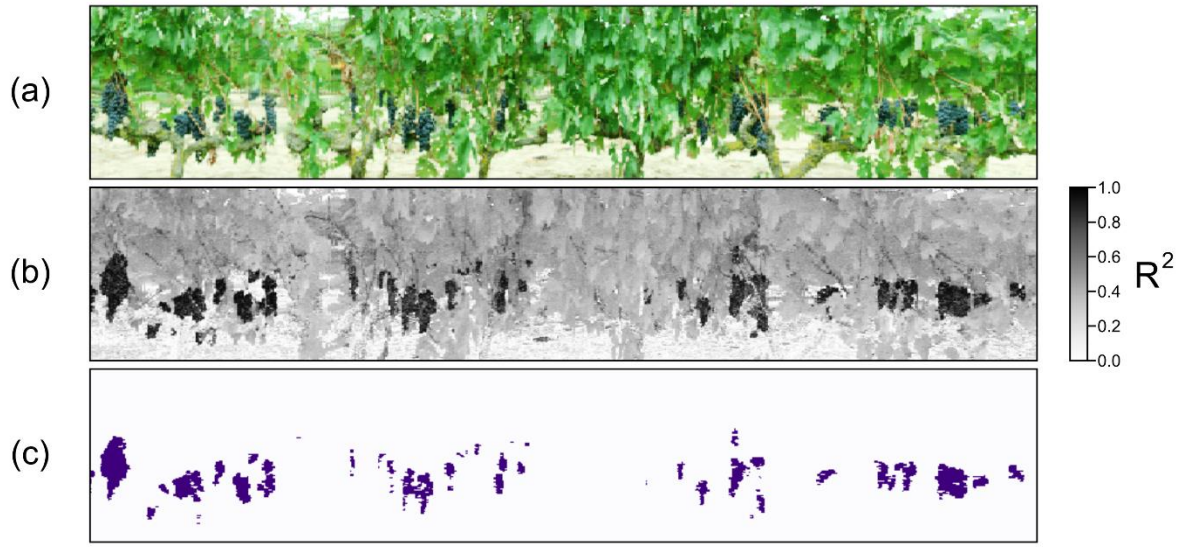

576

577 **Fig 3** (a) Hyperspectral image from a block in RGB channels (histogram normalized for the sake of
578 illustration). (b) Correlation matrix with R^2 values between the pixel spectrum and a grape reference
579 spectrum. A Gaussian smoothing was applied with $\sigma = 1.0$. (c) Image with segmented grape pixels
580 (pixels in (b) whose $R^2 \geq 0.75$). All the images were stretched in the horizontal axis for aesthetic
581 purposes.

582

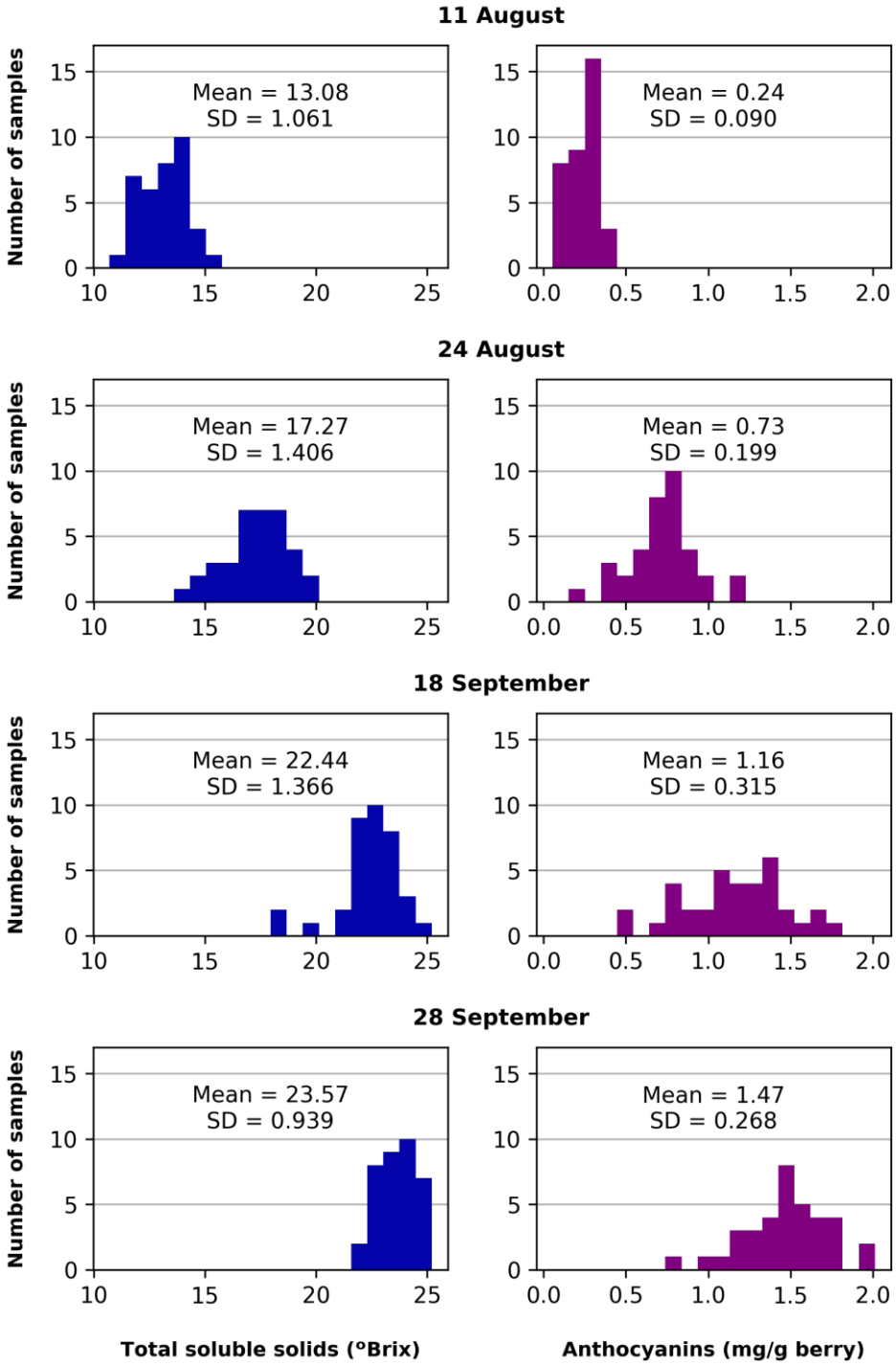

583

584 **Fig 4** Histograms for total soluble solids (left column) and anthocyanin concentrations (right column)
585 for each one of the experimental dates on 2017. SD: standard deviation.

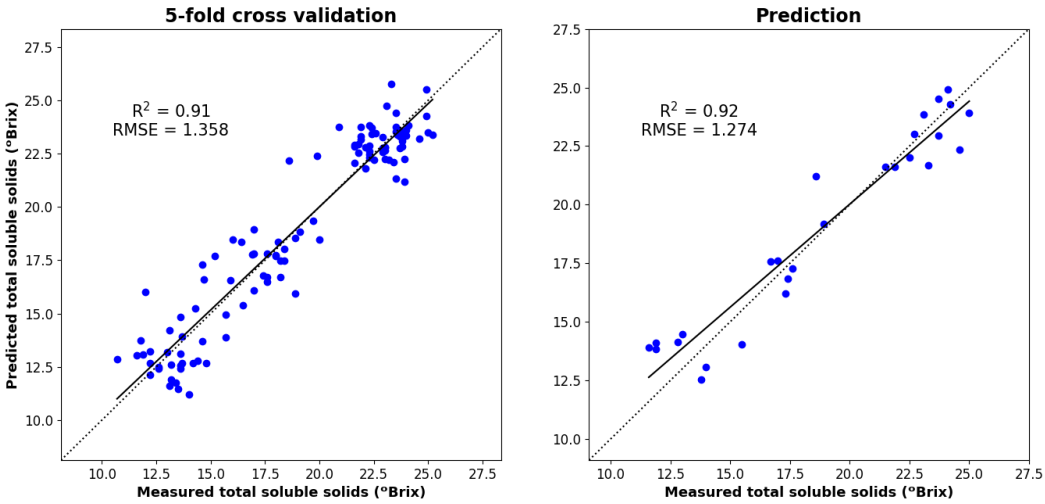

Fig 5 Regression plot for 5-fold cross validation (a) and prediction results (b) for the total soluble solids models. Solid closed line segment refers to the regression line of the samples, while the dotted open line segment represents the 1:1 trend. RMSE: root mean squared error (in ºBrix).

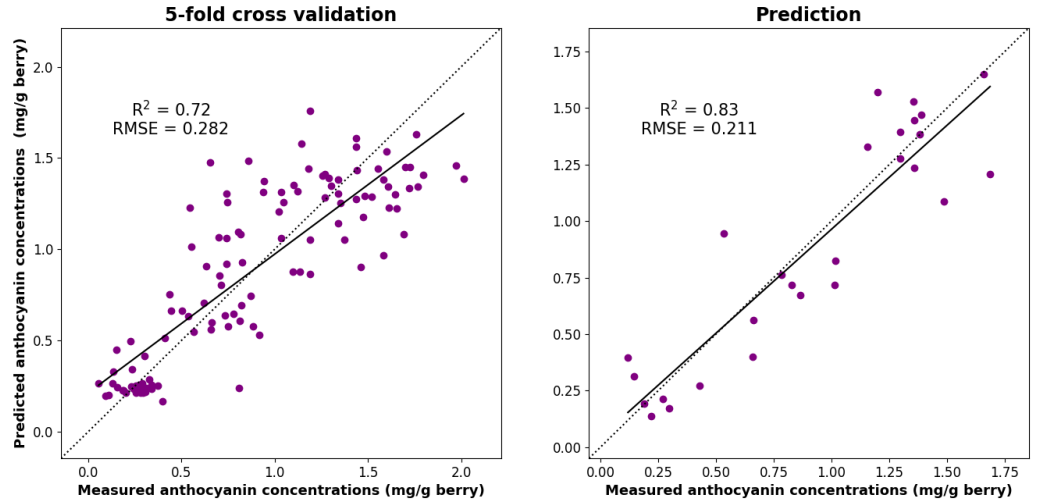

Fig 6 Regression plot for 5-fold cross validation (a) and prediction results (b) for the anthocyanins concentrations models. Solid closed line segment refers to the regression line of the samples, while the dotted open line segment represents the 1:1 trend. RMSE: root mean squared error (in mg/g berry).

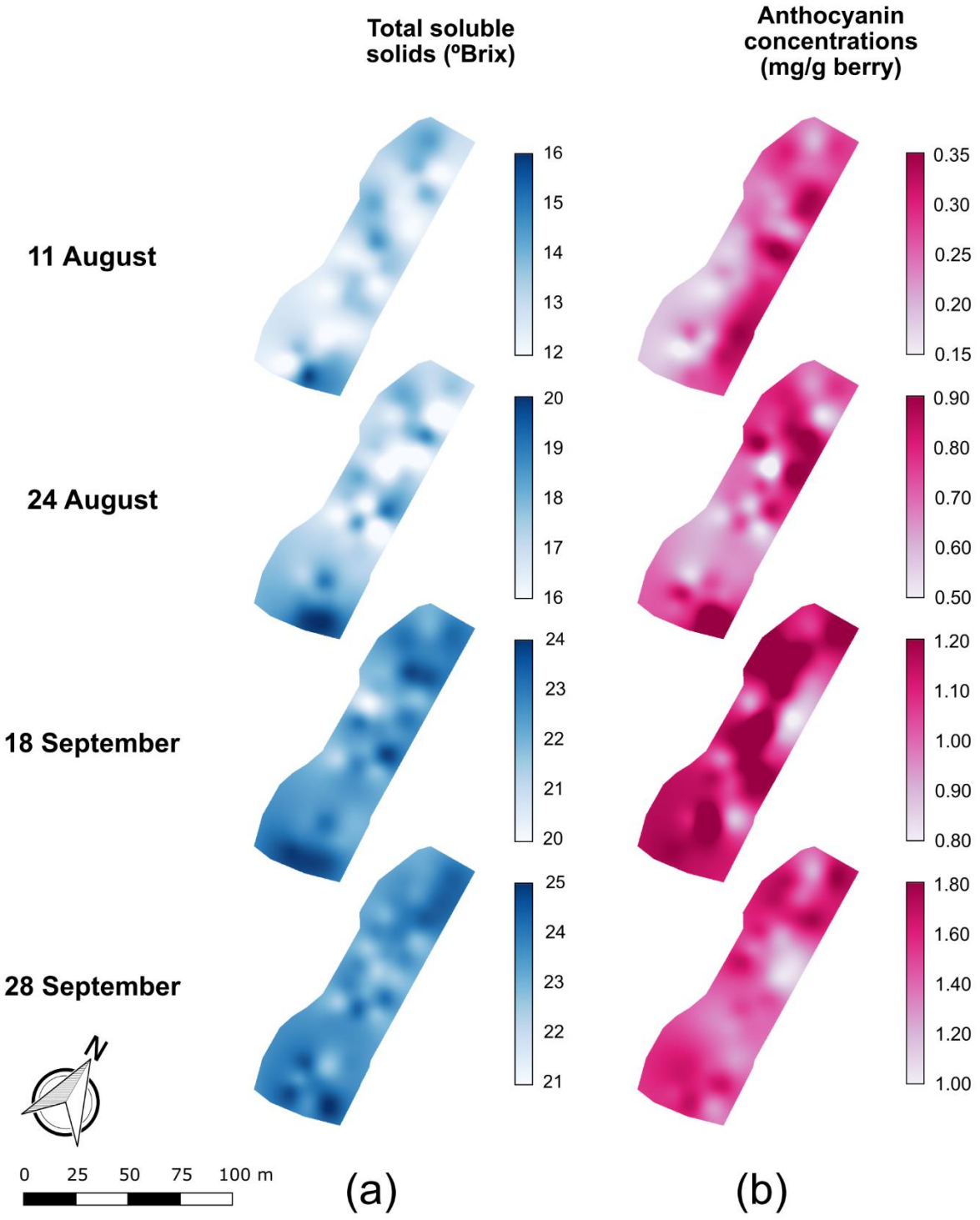

597

598 **Fig 7** Prediction maps for grape total soluble solids (a) and anthocyanin concentrations (b) displaying
599 the evolution of both parameters for the four different dates during grape ripening.